The effect of ternary alloying with vanadium on Ti-Pt shape memory alloys

P Daswa[1,2], S Chikosha[1,a], M L Mahlatji[1], C W Siyasiya[2]

[1]Light Metals Impact Area, Manufacturing Cluster, Council for Scientific and Industrial Research (CSIR), Meiring Naudé, Pretoria, South Africa

[2]Department of Materials Science and Metallurgical Engineering, University of Pretoria, Pretoria, South Africa

[a]SChikosha@csir.co.za

Abstract. Ti-Pt alloys have attracted much research due to high transformation temperatures (1050ºC) which makes them suitable for high temperature applications in automotive and aerospace industries. The binary alloy exhibits negligible shape memory effect and the amount of platinum (Pt) required to produce this alloy makes it very expensive which limits its practical application and commercialization. Ternary alloying of Ti-Pt could lead to solid solution strengthening and improved shape memory properties. Furthermore, ternary alloying by replacing Pt could reduce the cost of the alloy. However, it could lead to changes in the microstructure, crystal structure, transformation temperatures and transformation temperature hysteresis that would significantly affect the shape memory behaviour of the alloy. This paper investigates the effect of ternary alloying of Ti-Pt with varying vanadium contents (0-18.25 at.%) on the as-cast condition. The effect of ternary alloying on the microstructure, transformation temperature and transformation temperature hysteresis were studied. The Ti_{50}-Pt_{50-x}-V_x (x = 6.25 to 18.25 at.%) alloys were produced by the button arc melting method using elemental powders of titanium, platinum and vanadium. Results showed the formation of martensitic α-$Ti_{50}(Pt,V)_{50}$ with Ti_3Pt, $(Ti,V)_3Pt$, Ti_4Pt_3-like and oxide phases in Ti-Pt-(V) alloys. The phase transformation temperature of Ti-Pt alloys decreased with increasing vanadium content up to 10.2 at.% V.

1. Introduction

Shape memory alloys (SMA) are a type of smart material that have attracted much research in the automotive, biomedical, civil and aerospace industries [1,2,3]. They display a peculiar capability of recovering large deformations upon heating through a reversible martensitic transformation that enables them to generate an actuating force [1,2]. This characteristic makes SMAs very attractive for actuating applications in aerospace, automotive and biomedical industries.

Ti-Ni, the most successfully commercialized SMA, has been used for varying applications due to its excellent properties such as superelasticity, shape memory property, biocompatibility and good corrosion resistance [4, 5]. However, it is limited to lower temperature applications of less than 100ºC due to its related low transformation temperatures [4-5]. Although research had proposed that alloying of the binary alloy system could be used as an alternative way of increasing the transformation temperature, the maximum martensitic transformation temperatures for the Ti-Ni based alloys achieved to date still remain below 750ºC [1,6–8]. This still limits their application in the aerospace industry. The Ti-Pt alloy has been suggested as a high temperature shape memory alloy due to its high martensitic transformation temperature of about 1050ºC [9]. It undergoes a cubic austenitic B2 to an orthorhombic

martensitic B19 phase transformation. Ti-Pt alloys exhibit negligible shape memory effect and the high cost of Pt could limit the practical application of these alloys. Ternary alloying of Ti-Pt alloys by substituting Pt with a cheaper element has attracted research as this could be an alternative of improving the shape memory behavior of Ti-Pt alloys to improve work output (actuating ability) and reduce cost of the alloys [10-12]. Chikosha *et al*. [12] investigated the effect of ternary alloying Ti-Pt alloys with vanadium replacing Pt by 6.25 at.% V. They reported that the transformation temperature decreased by the addition of 6.25 at.% V in the alloy. None of the published work has considered the effect of adding varying contents of vanadium and its effect on transformation temperature. Therefore, this study investigated the effect of ternary alloying with varying vanadium contents (0-18.25 at.% V) on the microstructure and transformation temperature of as-cast Ti-Pt shape memory alloys.

2. Experimental Procedure

Elemental powders of high purity Ti grade 1 (99.9 %), Pt (99.9 %) and V (99. 5%) were prepared in desired quantities to achieve homogeneous powder blends with compositions: Ti_{50}-Pt_{50}, Ti_{50}- $Pt_{43.75}$-$V_{6.25}$, Ti_{50}-$Pt_{37.5}$-$V_{12.5}$ and Ti_{50}-$Pt_{31.25}$-$V_{18.75}$ (at.%). Ti elemental powder was sourced from TLS, Technik, GmbH & Co, Germany. LGC Industrial Analytical (Pty) Ltd, South Africa, supplied the Pt and V elemental powders. The powder blends were cold compacted at room temperature using an ENERPAC VLP 100 tonne press at 2842 MPa (100 bars) with a die size of 10 mm diameter to produce green compacts. The green compacts were then arc-melted in an argon atmosphere to produce 10 mm diameter alloy buttons. In order to achieve homogeneity, the binary Ti-Pt compact was remelted three times and the ternary Ti_{50}-Pt_{50-x}-V_x compacts were remelted six times. All the characterisation and analysis was conducted on as-cast samples. Metallographic analysis was done on the sectioned, mounted and polished as-cast samples. Scanning electron microscopy (SEM) with an energy-dispersive X-ray spectrometer (EDS), using a JEOL JSM-6510 instrument was used to determine microstructure, composition and phases of the alloys. Differential scanning calorimetry (DSC), using a Netzsch STA449F3 was done to investigate the thermal behaviour such as transformation temperatures, hysteresis and latent heats of transformation. The heating and cooling rate was 20^{o}C/min and the temperature range was from room temperature to 1400^{o}C Samples were subjected to two thermal heating and cooling cycles.

3. Results and Discussion

Figures 1-4 show SEM backscattered electron images (BEI) and EDX results of Ti_{50}-Pt_{50}, Ti_{50}-$Pt_{43.75}$-$V_{6.25}$, Ti_{50}-$Pt_{37.5}$-$V_{12.5}$ and Ti_{50}-$Pt_{31.75}$-$V_{18.25}$ alloys in the as-cast condition. The chemical compositions shown for all phases are the average values taken from three different sections of the sample. The overall compositions (Figures1-4) were slightly different from the initial measured compositions, but the difference is within the error margin of EDX measurements. However, they were still within the TiPt single phase region [13].

The resultant microstructures were inhomogeneous and consisted of at least three contrast areas. All of the alloys followed a similar solidification sequence during cooling. On solidification, above the eutectic temperature, the alloy consisted of the liquid and β-TiPt dendrites. At the eutectic temperature, the residual liquid transformed to the eutectic Ti_3Pt and β-TiPt phases. Below the peritectoid temperature, the β-TiPt dendrites disintegrated into Ti_4Pt_3 at the β-TiPt/interdendritic interface which grew towards the core of the dendrite [14]. At low martensitic transformation temperature, the β-TiPt in the dendrite and interdendritic regions transformed to the low temperature α-TiPt phase. The formation of an oxide phase in Ti_{50}-Pt_{50} and Ti_{50}-$Pt_{31.75}$-$V_{18.25}$ was observed. The latter is stabilised by oxygen picked up during sample processing [15,18].

Binary Ti-Pt was comprised of α-TiPt, which transformed martensitically from primary β-TiPt dendrites, and an interdendritic region with Ti_4Pt_3, oxide phase suspected to be Ti_3Pt (stabilised by oxygen) and α-TiPt (Figure 1).

The Ti_{50}-$Pt_{43.75}$-$V_{6.25}$ alloy consisted of α-Ti(Pt,V) dendrites and the interdendritic regions were comprised of $(Ti,V)_4Pt_3$ and Ti_3Pt phases (Figure 2). The EDX results from the SEM revealed that the transforming Ti(Pt,V) phase contained 5.8 at.% V.

The Ti_{50}-$Pt_{37.5}$-$V_{12.5}$ alloy consisted of α-Ti(Pt,V) dendrites while the interdendritic regions were composed of Ti_4Pt_3 and Ti_3Pt phases (Figure 3). It was suspected that the Ti_4Pt_3 phase has vanadium substituting for both Ti and Pt, its full characterisation is part of ongoing work. The EDX results from the SEM revealed that the transforming Ti(Pt,V) phase contained 10.2 at.% V.
The Ti_{50}-$Pt_{31.75}$-$V_{18.25}$ alloy had the most complex microstructure, consisting of Ti_4Pt_3 and oxide phase dendrites interspersed with a low volume fraction of Ti(Pt,V) phase in the interdendritic regions (Figure 4). During solidification, the alloy consist of liquid and β-TiPt dendrites above eutectic temperature and the liquid further transforms to the Ti_3Pt + β-TiPt eutectic at the eutectic temperature. Below the peritectoid temperature, the β-TiPt dendrites transform partitionlessly to Ti_4Pt_3 upon cooling [14]. The β-TiPt phase in the eutectic transforms to α-TiPt at the martensitic transformation temperature. The EDX results showed that the Ti(Pt,V) phase formed contained only 8.2 at.% V which is far off from the intended composition of 18.25 at.% V, as such it will not be reported on further.
The volume fraction of the interdendritic regions increased with increasing vanadium addition, thereby reducing volume fraction of the transforming TiPt phase. During transformation, the β-TiPt dendrite decomposed into $Ti_4(Pt,V)_3$ and α-TiPt. However, with the higher contents of vanadium, the transformation of $Ti_4(Pt,V)_3$ was favoured and resulted in the low volume fraction of the TiPt phase in Ti_{50}-$Pt_{31.25}$-$V_{18.25}$.

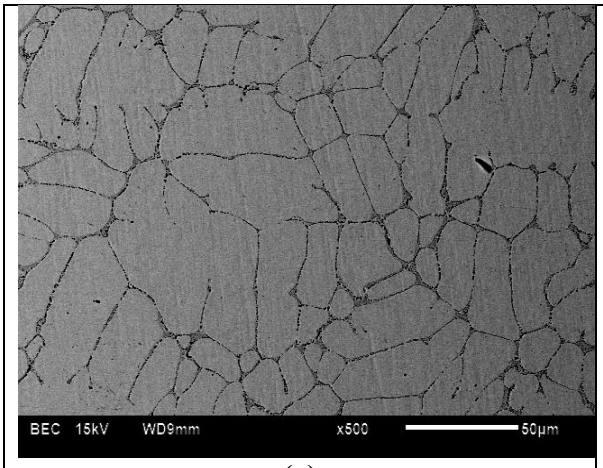

(a)

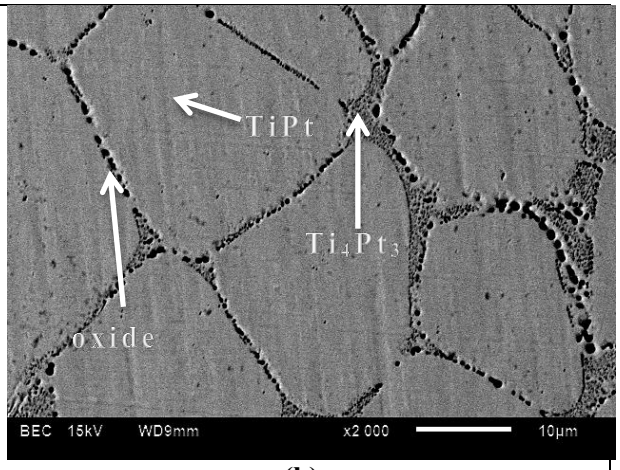

(b)

	O-K		Ti-K		Pt-K	
	wt%	at.%	wt%	at.%	wt%	at.%
Overall	-	-	20.5±0.1	51.3±0.3	79.5±0.3	48.7±0.2
TiPt	-	-	20.0±0.3	50.5±0.7	80.0±0.5	49.5±0.3
Ti_4Pt_3	-	-	24.0±0.5	56.3±1	76.0±0.8	43.7±0.5
oxide	15.7±0.9	44.0± 2	51.7±0.4	48.5±0.3	32.6±0.3	7.5±0.1

Figure 1. SEM backscattered electron images (BEI), (a) low and (b) high magnification with EDX results of Ti_{50}-Pt_{50} in the as-cast condition.

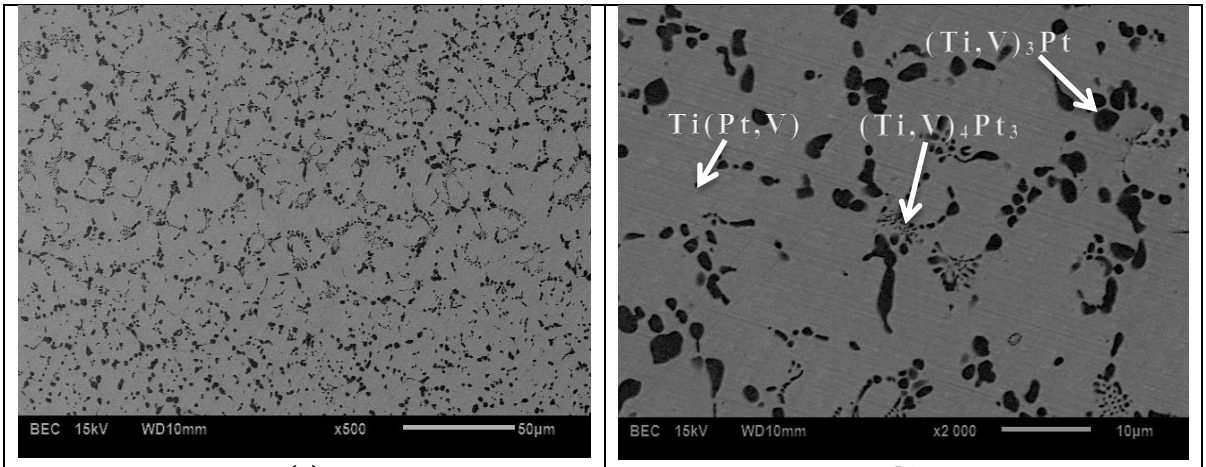

(a) **(b)**

	Ti-K		V-K		Pt-K	
	wt%	at.%	wt%	at.%	wt%	at.%
Overall	21.8±0.2	50.7±0.4	2.9±0.1	6.4±0.2	75.3±04	42.9±02
Ti(Pt,V)	20.6±0.4	49.1±-1	2.6±0.22	5.8±0.5	76.8±0.7	45.1±0.4
$(Ti,V)_4Pt_3$	21.6±0.2	50.28±0.6	2.9±0.2	6.4±0.4	75.5±0.4	43.3±0.3
$(Ti,V)_3Pt$	38.6±0.6	67.5±0.9	5.1±0.5	8.4±0.8	56.2±0.7	24.1±0.3

Figure 2. SEM backscattered electron images (BEI), (a) low and (b) high magnification with EDX results of Ti-$Pt_{43.75}$-$V_{6.25}$ in the as-cast condition.

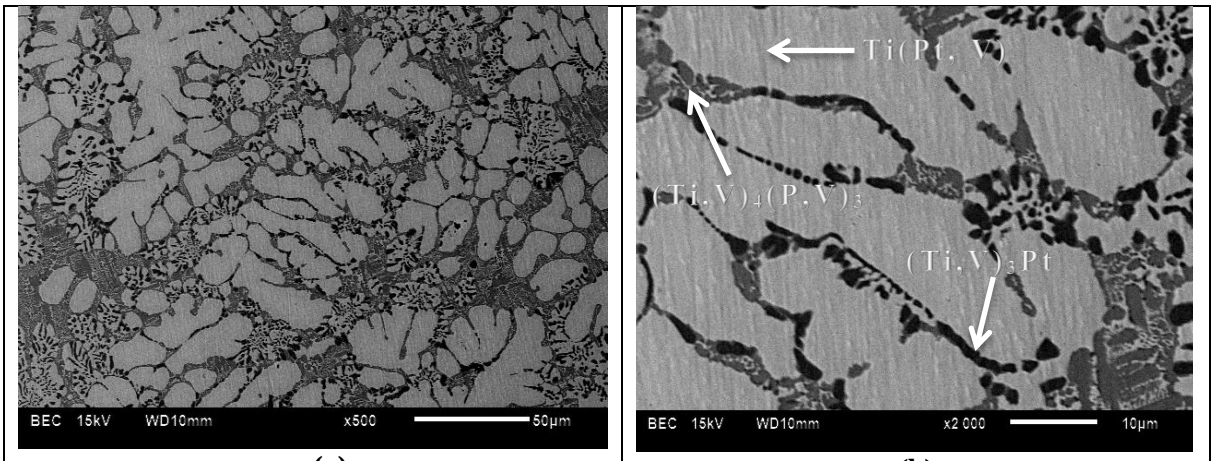

(a) **(b)**

	Ti-K		V-K		Pt-K	
	wt%	at.%	wt%	at.%	wt%	at.%
Overall	24.4± 0.1	51.4±0.2	6.5±0.1	12.9±0.2	69.1±0.2	35.8±-0.1
Ti(Pt,V)	22.1±0.3	49.5±0.7	4.8±0.2	10.2±0.4	73.1±0.5	40.3±0.3
$(Ti,V)_4(Pt,V)_3$	22.6±0.3	42.2±0.6	17.1±0.3	30.1±0.6	60.3±0.5	27.7±0.2
$(Ti,V)_3Pt$	38.6±0.4	67.9±0.6	4.5±0.2	7.5±0.4	56.9±0.5	24.6±0.2

Figure 3. SEM backscattered electron images (BEI), (a) low and (b) high magnification with EDX of Ti-$Pt_{37.5}$-$V_{12.5}$ in the as-cast condition.

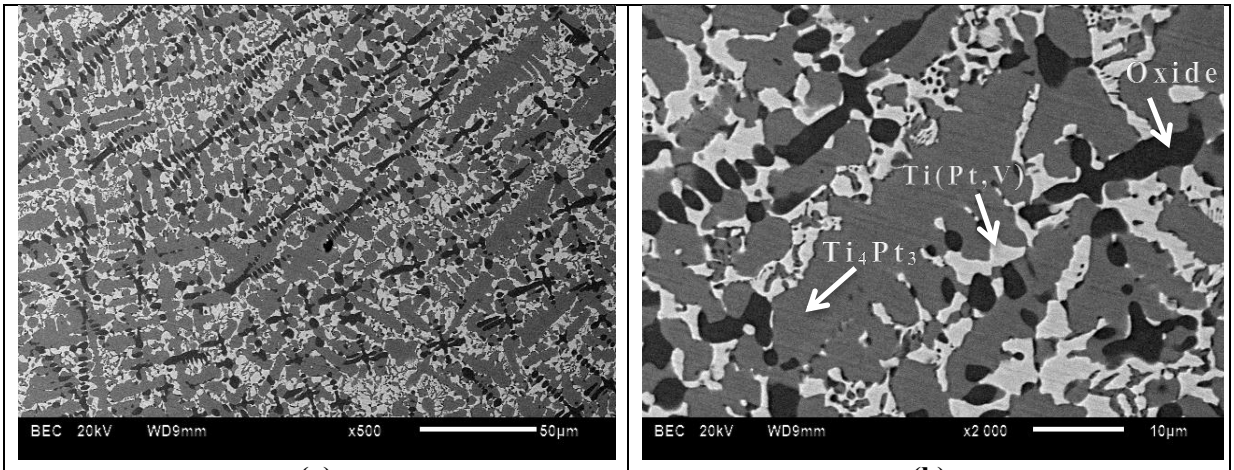

(a) **(b)**

	O-K		Ti-K		V-K		Pt-K	
	wt%	at.%	wt%	at.%	wt%	at.%	wt%	at.%
Overall			25.6±0.1	50.2 ±0.3	10.2 ±0.1	18.9± 0.2	64.2± -1	30.9±0.5
Ti(Pt, V)	-	-	23.7± 0.5	51.4±1.1	3.9±0.4	8.2±0.8	72.4±0.4	40.4±1.9
$(Ti,V)_4(Pt,V)_3$	-	-	22.2± 0.4	41.4±0.7	17.7±0.4	31.1±0.7	60.1±4.3	27.5±2
oxide	8.3±0.5	32.4 ± 2	34.4± 0.5	44.8±0.8	5± 0.3	6.1±0.4	52.3±4	16.7±1.3

Figure 4. SEM backscattered electron images (BEI), (a) low and (b) high magnification with EDX of Ti-$Pt_{31.75}$-$V_{18.25}$ in the as-cast condition

The SEM-EDX results revealed that the exact compositions of the transforming TiPt phases deviated from the intended compositions as follows: The Ti_{50}-Pt_{50} sample formed $Ti_{50.5}Pt_{49.5}$, the Ti_{50}-$Pt_{43.75}$-$V_{6.25}$ sample formed $Ti_{49.1}(Pt_{45.1},V_{5.8})$, the Ti_{50}-$Pt_{37.5}$-$V_{12.5}$ sample formed $Ti_{49.5}(Pt_{40.3},V_{10.2})$, and the Ti_{50}-$Pt_{31.75}$-$V_{18.25}$ sample formed $Ti_{51.4}(Pt_{40.4},V_{8.2})$. Due to the large deviation of the transforming phase from the intended composition in the Ti_{50}-$Pt_{31.75}$-$V_{18.25}$ sample, its DSC result was not presented. Furthermore, its transformation temperatures did not vary significantly from those of $Ti_{49.5}$-$Pt_{40.33}$-$V_{10.2}$.

Figure 5 shows two heating and cooling DSC cycles of the as-cast Ti-Pt alloy. The first heating segment displayed a single step reverse transformation labelled M→A, with austenite start and finish temperatures of A_s = 1031.8°C and A_f = 1046.5°C. During cooling, the forward transformation was believed to proceed via a multi-stage transformation sequence, similar to what was observed by Biggs *et al.* and proposed that the behaviour was analogous to the Ni-Ti system [13,14]. The first cooling peak, labelled A→M_1, with martensite start and peak temperatures of M_s = 992.3°C and M_p = 983.2°C was the partial transformation of austenite to B19 martensite phase. On further cooling, the remaining austenite transformed into an unidentified intermediate phase (I) in a reaction characterised by a peak temperature I_p of 971.0°C. With further cooling, the intermediate phase transformed into a B19 martensite phase according to the reaction I→M_2 with peak and finish temperatures of M_p = 951.5°C and M_f = 935.7°C. On the contrary, Karem [14] reported the occurrence of a decomposition reaction of β-TiPt phase below the peritectoid isotherm into Ti_4Pt_3 and Pt-enriched β-TiPt. It is not yet clear whether such decomposition reaction takes place in the present alloy, but if it does, it would account for the intermediate exothermic peak attributed to the A→I reaction. In this case, the Pt-rich decomposition β-TiPt product would transform to martensite at a slightly lower temperature. Further work is required to fully understand the mechanism behind this observed transformation sequence.

The second heating segment proceeded through two steps. Based on the intermediate theory analogous to the Ti-Ni system, the first peak was reverse transformation of the B19 martensite (M_2) into austenite, M_2→A, followed by reverse transformation of B19 martensite (M_1) in the reaction M_1→A. The characteristic transformation temperatures and thermal hysteresis of the second cycle heating M_1→A transformation were close to those of the first cycle heating M→A transformation (Figure 5 and Table

1). This was an indication that the martensite types M and M_1 comprised martensite variants of similar characteristics, most likely forming freely within dendrites in a similar manner to Ti-Ni [16]. The reaction $M_2 \rightarrow A$ was associated with the forward reaction $A \rightarrow I \rightarrow M_2$. Similarly, the B2→B19′ transformation in Ni-Ti alloys can also be supressed by conditions such as compositional inhomogeneity, local stress fields around precipitates and high density dislocation networks produced by thermomechanical treatments [13-14]. This changes the transformation sequence to B2→R→B19′, where the R-phase is a trigonal-like martensite phase that forms in competition with the monoclinic B19′ phase.

The thermal hysteresis was defined as the difference between the forward (A→M) and reverse (M→A) transformation temperatures using equation [18]:

$$\Delta T = Af - Ms \quad (1)$$

A thermal transformation hysteresis of ΔT = 65.7°C on the first cycle and 60.7°C on the second cycle was achieved. This was higher than previously reported for Ti-Pt [19]. The transformation enthalpies of the forward and reverse transformations were not easily discernible due to the overlapping of intermediate phase peaks. The exception was the reverse transformation on the first cycle where the transformation enthalpy was determined -33.2J/g, which was higher than reported for Ti-Pt [19].

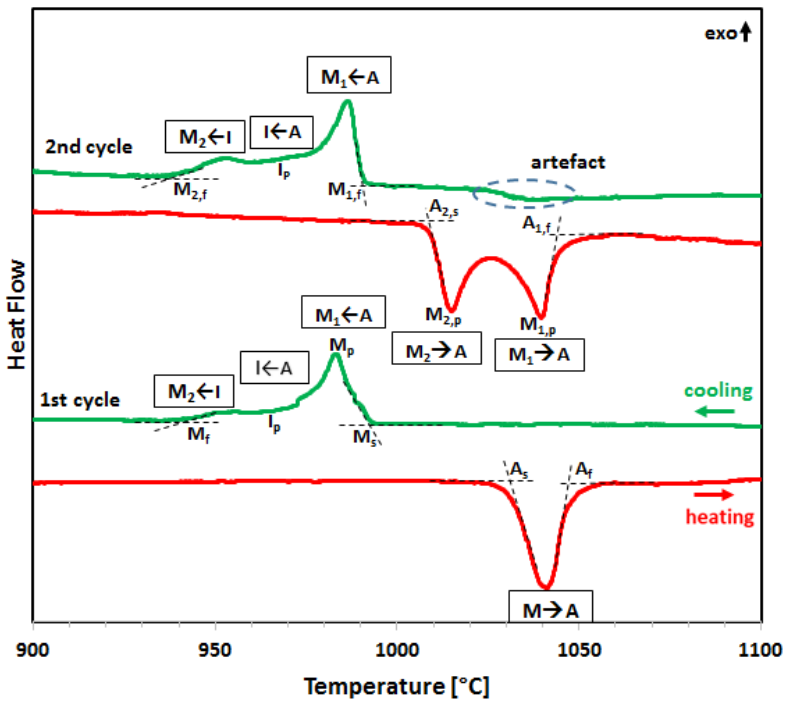

Figure 5. Two DSC cycles of as-cast Ti-Pt alloy sample showing the transformation temperatures of the $Ti_{50.5}Pt_{49.5}$ (at.%) phase. A = B2 Austenite. M = B19 Martensite. I = Intermediate

Table 1. Transformation temperatures of $Ti_{50.5}Pt_{49.50}$ phase during heating and cooling for two DSC thermal cycles.

Transformation Temperatures (^{0}C) Heating				**Transformation Temperatures (^{0}C) Cooling**				
Cycle 1								
	M→A start	M→A peak	M→A finish	A→M_1 start	A→M_1 peak	A→I peak	I→M_2 peak	I→M_2 finish
	1031.8	1040.8	1046.5	992.3	983.2	971.0	951.5	935.7
Cycle 2								
M_2→A start	M_2→A peak	M_1→A peak	M_1→A finish	A→ M_1 start	A→ M_1 peak	A→I peak	I→M_2 peak	I→M_2 finish
1009.5	1014.7	1039.6	1043.5	993.1	986.5	971.9	952.6	937.7

Figure 6 shows DSC second cycle curves of Ti-Pt_{50-x}-V_x phase (x = 0, 5.8 and 10.2 at.% V). The binary Ti-Pt second cycle curve was replotted for ease of comparison. First and second cycle heating curves for $TiPt_{50-x}V_x$ phase (x = 5.8, 10.2) did not display significant variation, so only second heating cycle results were plotted. Ternary alloying of Ti-Pt with V by replacing Pt changed the transformation from multiple to single step and reduced the martensitic transformation temperatures. The M_s temperatures decreased from 992°C (binary Ti-Pt) to 925°C for $Ti_{49.1}$-$Pt_{45.1}$-$V_{5.8}$ and 820°C for $Ti_{49.5}$-$Pt_{40.33}$-$V_{10.2}$. The reduction in transformation temperatures was predicted by first principles calculations, which showed that ternary alloying of V to Ti-Pt alloy promoted the stability of the B2 phase by increasing the C′ shear modulus, thus decreasing the transformation temperature [20]. This was in agreement with transformation temperature reduction trends observed in ternary alloying when Ni was partially substituted with V, Cr, Mn, Fe or Co in Ni-Ti alloys [3,4].

The $Ti_{49.1}(Pt_{45.1},V_{5.8})$ phase showed no significant difference on the start and finish temperatures of the reverse transformation. However, it significantly depressed the forward transformation, widening the transformation hysteresis to ΔT = 142.2°C. The $Ti_{49.5}(Pt_{40.3},V_{10.2})$ phase resulted in further widening of the thermal hysteresis to ΔT = 191.4°C. This would be a disadvantage in actuation applications where narrow thermal hysteresis is required for fast response times [3].

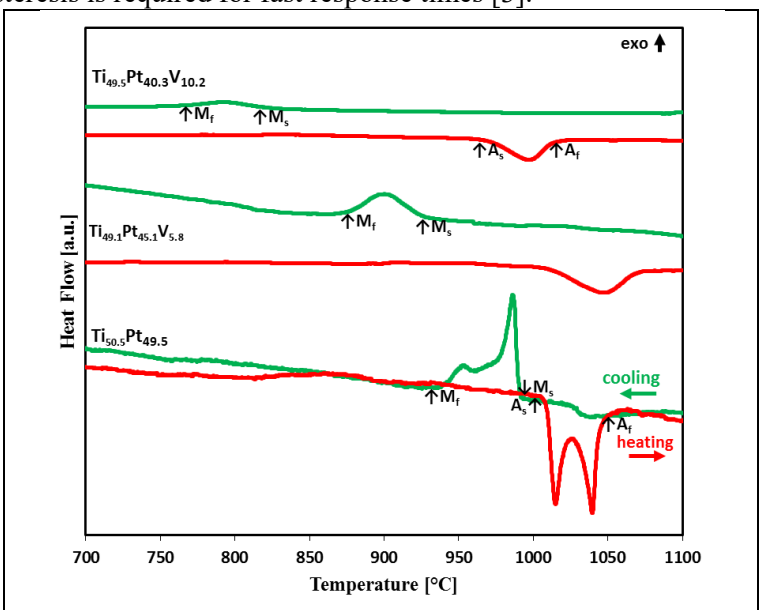

Figure 6. Second cycling DSC curves of as-cast $Ti_{50}Pt_{50}$, Ti_{50}-$Pt_{43.75}$-$V_{6.25}$ and Ti_{50}-$Pt_{37.5}$-$V_{12.5}$ (at.%) alloy samples showing the transformation temperatures of the $Ti_{50.5}Pt_{49.5}$, $Ti_{49.1}(Pt_{45.1},V_{5.8})$, $Ti_{49.5}(Pt_{40.3},V_{10.2})$ (at.%) phases.

Table 2. Transformation temperatures and hysteresis of second thermal cycles on $Ti_{49.1}$-$Pt_{45.1}$-$V_{5.8}$ and $Ti_{49.5}$-$Pt_{40.3}$-$V_{10.2}$ phases of as-cast Ti_{50}-$Pt_{43.75}$-$V_{6.25}$ and Ti_{50}-$Pt_{37.5}$-$V_{12.5}$ (at.%) alloy samples.

Phase	A_s (°C)	A_f (°C)	M_s (°C)	M_f (°C)	ΔT (°C)
$Ti_{49.1}$($Pt_{45.1}$,$V_{5.8}$)	1012.2	1067.4	925.0	878.0	142.4
$Ti_{49.5}$($Pt_{40.3}$,$V_{10.2}$)	974.6	1011.4	820.0	766.9	191.4

Ternary alloying of Ti-Pt by substituting Pt with varying contents of vanadium resulted in the formation of an inhomogeneous microstructure with different phases in the dendrites and inter-dendritic regions. The binary Ti-Pt alloy showed multiple transformation peaks due to intermediate phases being confined to interdendritic regions. The addition of V changed the transformation sequence from multiple steps to single step transformation, lowered the transformation temperature and widened the transformation hysteresis. Although the martensitic transformation temperatures of $Ti_{49.1}Pt_{45.1}V_{5.8}$ and $Ti_{49.5}Pt_{40.3}V_{10.2}$ phases were decreased, they were still above 750 °C. Therefore, these alloys could still be potentially used for high temperature shape memory applications (>750°C), while lowering cost by reducing the Pt content.

4. Conclusions

- Multiple phases were observed in as-cast Ti-Pt-V alloys.
-The amount of transforming Ti(Pt,V) phase formed reduced with increasing vanadium content.
-Binary Ti-Pt showed multiple thermal transformation peaks, this changed to single step transformation in ternary Ti_{50}-Pt_{50-x}-V_x.
- The addition of vanadium reduced the transformation temperatures of the Ti-Pt alloy and increased transformation hysteresis.
- Transformation temperatures higher than 750°C were achieved in alloy with 10.2 at.% V, retaining potential for high temperature applications.

5. References

[1] Saghaian S M, Karaca H E, Souri M, Turabi A S and Noebe R D 2016 Tensile shape memory behavior of $Ni_{50.3}Ti_{29.7}Hf_{20}$ high temperature shape memory alloys *Mater. Des.* **101** 340–5
[2] Mamiko K, Madoka T, Satoshi T and Yoko Y-M 2012 Effect of Zr on phase transformation and high temperature shape memory effect in TiPd alloys *Mater. Lett.* **89** 336–8
[3] Kamila S 2013 Introduction, classification and applications of smart materials: An overview *Am. J. Appl. Sci.* **10** 876–80
[4] Hee Y K, Tatsuhito F, Pio John B, Tae-Hyun N and Shuichi M 2011 Martensitic transformation and shape properties of Ti-Ta-Sn high temperature shape memory alloys *Mater. Sci. Eng.* A **528** 7238–46
[5] Ma L W, Cheng H S, Cao C W and Chung C Y 2012 Study of thermal scanning rates on transformations of Ti-19Nb-9Zr (at.%) by means of Differential Scanning Calorimetry analysis *J. Mater. Eng. Perform.* 2675–9
[6] Rios O, Noebe R, Biles T, Garg A, Palczer A, Scheiman D, Seifert H J and Kaufman M 2005 Characterization of ternary NiTiPt high-temperature shape memory alloys *Smart Structures and Materials 2005: Active Materials: Behavior and Mechanics* vol 5761 p 376
[7] Karakoc O, Hayrettin C, Bass M, Wang S J, Canadic D, Mabe J H, Lagoudas D C and Karaman I 2017 Effects of upper cycle temperature on the actuation fatigue response of NiTiHf high temperature shape memory alloys *Acta Mater.* **138** 185–97
[8] Canadinc D, Trehern W, Karaman I, Sun F and Chaudhry Z 2019 Ultra-high temperature multi-component shape memory alloys *Scr. Mater.* **158** 83–7
[9] Biggs T, Cortie M B, Witcomb M J and Cornish L A 2001 Martensitic Transformations , Microstructure , and Mechanical Workability of TiPt *Metall. Mater. Trans.* A **32** 1881–6
[10] Yamabe-Mitarai Y, Arockiakumar R, Wadood A, Suresh K S, Kitashima T, Hara T, Shimojo M, Tasaki W, Takahashi M, Takahashi S and Hosoda H 2015 Ti(Pt, Pd, Au) based high temperature shape memory alloys *Mater. Today Proc.* S **2** 517–22

[11] Bozzolo G, Mosca H O and Noebe R D 2007 Phase structure and site preference behavior of ternary alloying additions to PdTi and PtTi shape-memory alloys *Intermetallics* **15** 901–11
[12] Chikosha S, Mahlatji M, Modiba R and Chikwanda H 2018 The effect of vanadium on structure and martensitic transformation temperature of TiPt alloy *Conference of the South African Advanced Materials Initiative (COSAAMI-2018)*
[13] Biggs T, Cornish L A, Witcomb M J and Cortie M B 2004 Revised phase diagram for the Pt-Ti system from 30 to 60 at.% platinum *J. Alloys Compd.* **375** 120–7
[14] Karem E T A 2012 *Phase transformations and equilibria of titanium platinum alloys the composition range 30-50 atomic percent platinum*
[15] Lin H-C, Lin K M, Lin C-S and Chang S K 1999 A study of TiNiV ternary shape memory alloys *J. Alloys Compd.* **284** 213–7
[16] Otsuka K and Ren X 2005 Physical metallurgy of Ti-Ni based shape memory alloys *Prog. Mater. Sci.* **50** 511–678
[17] Liu Y and McCormick P 1996 Criteria of transformation sequence in NiTi shape memory alloys *Mater. Trans.* **37** 691–6
[18] Sehitoglu H, Hamilton R, Maier H J and Chumlyakov Y 2004 Hysteresis in NiTi alloys *J. Phys.* **IV** 3–10
[19] Rotaru G M, Tirry W, Sittner P, Van Humbeeck J and Schryvers D 2007 Microstructural study of equiatomic PtTi martensite and the discovery of a new long-period structure *Acta Mater.* **55** 4447–54
[20] Modiba R, Baloyi E, Chikosha S, Chauke H . and Ngoepe P E 2018 Computational modelling of Ti50Pt50Vx potential shape memory alloy *Conference of the South African Advanced Materials Initiative (COSAAMI-2018)*
[21] Wadood A, Takahashi M, Takahashi S, Hosoda H and Yamambe-Mitarai Y 2013 High temperature mechanical and shape memory properties of TiPt-Zr and TiPt-Ru alloys *Mater. Sci. Eng. A* **564** 34–41
[22] Tello K E, Noebe R D, Garg A, Allaz J and Kaufman M J 2017 Materials Characterization Revisiting the Ti-Pt system relevant to high temperature shape memory alloys **130** 97–104